Available online at www.sciencedirect.com
SCIENCE DIRECT®
ELSEVIER
Nuclear Instruments and Methods in Physics Research B 222 (2004) 593–600
NIM B
Beam Interactions with Materials & Atoms
www.elsevier.com/locate/nimb

Ion transmission and characterization of ordered nanoporous alumina

Alenka Razpet [a,*,1], Göran Possnert [a], Anders Johansson [a], Anders Hallén [b], Klas Hjort [a]

[a] *Division of Ion Physics, Ångström Laboratory, Box 534, Uppsala University, SE-751 21 Uppsala, Sweden*
[b] *Department of Microelectronics and IT, Royal Institute of Technology, Stockholm, Sweden*

Received 22 January 2004

Abstract

Ordered nanoporous alumina samples with a pore diameter of 70 nm, an array period of 100 nm and several thicknesses were considered as possible masks for pattern transfer by MeV ion lithography. A simple procedure for the sample alignment using a 2 MeV He^+ beam was utilized. The energy distributions of transmitted ions as well as backscattering spectra were studied in aligned and non-aligned orientations. The best transmission, comparable to the relative surface area covered by pores, was reached for 2 μm thick samples and was independent on ion species. Although the transmission for thicker membranes was generally lower, it significantly depended on the quality of each individual sample. The presented ion beam technique can therefore be used as a tool for the characterization of porous materials. The acceptance angle for transmission through pores and the effective atomic density of samples can be obtained from the experimental data and it is shown that nanoporous alumina can be used as a mask for MeV ion lithography.

PACS: 81.07.−b; 81.61.Dn; 82.80.Yc; 85.40.Hp
Keywords: Nanomaterials; Anodic alumina; RBS; Transmission; Characterization; Ion lithography; Pattern transfer

1. Introduction

One of the challenges in the production of nanomaterials is to create highly ordered nanodot and nanowire arrays in different materials. Most successful progress so far was done on chemical synthesis of nanoarrays using templates of self ordered nanoporous alumina membranes prepared by anodic oxidation of high purity aluminum [1–3]. Recently, a successful attempt to use nanoporous alumina as a mask for pattern transfer by ion beam implantation and selective chemical etching was reported by Matsuura et al. [4]. In their work, a 500 nm thick nanoporous alumina membrane was used as a mask during irradiation of a single crystal (1 0 0) $SrTiO_3$ by 200 and 500

* Corresponding author. Tel.: +386-1-58-85374; fax: +386-1-56-12335.
E-mail addresses: alenka.razpet@angstrom.uu.se, alenka.razpet@ijs.si (A. Razpet).
[1] On leave from Department for Low and Medium Energy Physics, Jožef Stefan Institute, Jamova 39, SI-1000 Ljubljana, Slovenia.

0168-583X/$ - see front matter
doi:10.1016/j.nimb.2004.03.072

keV Pt ions respectively, to produce a 150 nm deep ordered array.

For production of ordered structures with a high ratio between a pore length and its diameter (aspect ratio), ions with larger penetrations depths in the irradiated materials should preferably be chosen. In this case, a mask must be thicker to stop the ions which are hitting the solid material between pores. As the acceptance angle for the transmission is largely reduced already for few micrometer thick membranes, such masks are harder to align with respect to the incident beam. In a work of Rehn et al., approximately 2 μm thick alumina masks and 1 MeV Kr ions were used for the ion implantation in silicon wafer. The resulting ordered pattern did not, however, fully reproduce the mask structure. The transmission though the masks used was only between 1% and 3%, which was explained by a failure to completely open the pores in alumina after two step anodization [5]. Although nanoporous alumina membranes appeared to be nearly perfect as material for template based chemical synthesis [6], the results from implantation experiments indicate that this is not the case for MeV ion transmission. Similar conclusion was obtained from porosity characterization of alumina membranes with an ion beam [7]. Results based on the Rutherford backscattering spectrometry (RBS) studies were not consistent with the scanning electron microscope (SEM) image analysis. The discrepancy was explained by imperfections in the pore structure.

In this paper, ion transmission through nanoporous alumina was studied. Several samples with different thicknesses were investigated using a 2 MeV He^+ beam. The membranes were carefully aligned relative to the beam to obtain the maximal transmission through the pores. The energy distributions of transmitted ions as well as conventional RBS spectra were measured at different orientations. Since the thickness of the thinnest alumina films used was not sufficient to stop 2 MeV He^+ ions, the transmission was also measured for a 3 MeV O^+ beam with a smaller penetration depth. It is described how an ion beam can be used for characterization of nanoporous alumina and it is also shown that this material is a promising template for MeV ion lithography.

2. Experimental methods

2.1. Fabrication of nanoporous alumina membranes

The samples were prepared by anodization of 0.5 mm thick high purity aluminum foils (Puratronic®, 99.998% from Alfa Aesar) following the procedure of Masuda and Fukuda [3]. The foils were first roughly polished and annealed for 3 h in nitrogen atmosphere at 400 °C to minimize mechanical stress. The annealing was followed by fine electro polishing for 3 min at constant voltage of 20 V in a 1:4 volume ratio mixture of perchloric acid and ethanol, resulting in surface roughness of about 5 nm. Two step anodization was performed in 0.3 M oxalic acid at constant voltage of 40 V and rigorous stirring at temperature of 1 °C. The anodization time was 24 h for the first step. The formed alumina was then etched off in a solution containing 1.8% CrO_3 and 5% H_3PO_4 for 12 h at room temperature. The second anodization step was done under the same conditions as the first step, but the anodization time was adjusted to obtain the desired thickness. For fabrication of the membranes used in this work, anodization times of 1 and 5 h were used in the second step, producing membranes with thicknesses of 2 and 10 μm, respectively. The remaining aluminum layer was removed by saturated $HgCl_2$ solution. The alumina film was carefully picked from the mercury chloride solution using a nylon mesh. Pore ends were opened in a 5% H_3PO_4 solution after 1 h. The samples were finally cleaned in deionised water.

2.2. Sample characterization

The characterization was performed at the Tandem Laboratory at Uppsala University using a 2 MeV He^+ beam collimated to a spot size with a diameter of ~2 mm. The beam current measured on the target was about 2 nA. Alumina samples with thicknesses of 2, 7 and 10 μm were investigated. Membranes were first glued to brass frames with a 3 mm central hole and attached to a sample wheel controlled by a precision goniometer in the experimental vacuum chamber. The sample could be rotated around two independent axes perpendicular to the ion beam direction. Sample wheel

movement was fully computer controlled by a scanning code originally developed for RBS channeling studies. The experimental setup is presented in Fig. 1.

The ion transmission was measured by a simple analyzing system consisting of a thin (~10 nm) gold target on a carbon backing and Detector 2 placed at the backscattering angle behind the sample wheel. By detection of backscattered ions from the gold target rather than transmitted ions directly, the high rate of incident particles that might destroy the silicon detector was largely reduced. The energy distribution of transmitted ions was obtained from the RBS spectra measured by Detector 2. The Rutherford scattering yield per energy interval $N(E_i)$ is proportional to I_t/E_i^2, where I_t is the transmitted current and E_i the energy of the transmitted ion. To obtain the number of counts per channel proportional to I_t, the energy dependence was eliminated from the relation by multiplying measured scattering yield at an energy E_i by $(E_i/E_0)^2$ where E_0 is the energy of the incident beam. The yield from scattering on the carbon backing and the effects causing the energy spread were neglected in this conversion. Conventional RBS spectra of the samples were also recorded with Detector 1 set at the scattering angle of 168° to obtain additional information about nanoporous alumina.

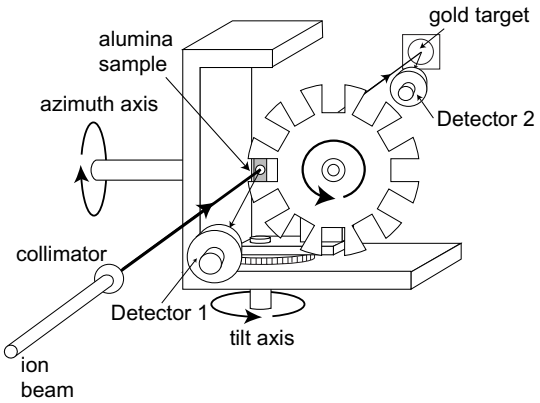

Fig. 1. Experimental setup used for the analysis. Detector 1 – the standard RBS detector, Detector 2 – the RBS detector for transmitted ions.

3. Results

A SEM image of a nanoporous alumina sample labeled A30 is displayed in Fig. 2. The thickness of the sample was determined from the cross section image (Fig. 2(b)). As can be seen, the pores extended through the entire depth and no geometrical differences between the front and the rear side were observed. The same was noted for most of the samples except for A39a where high purity aluminum from a different manufacturer (Goodfellow), but of the same purity was used for the anodization. The SEM image revealed that the pore ends were not opened completely after 1 h of etching in the H_3PO_4 solution.

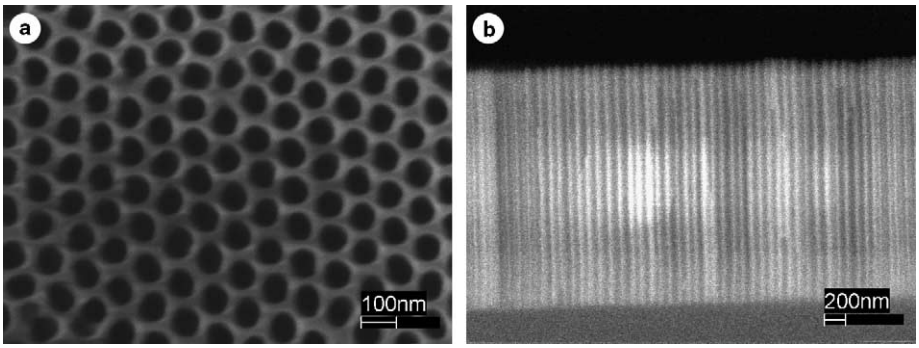

Fig. 2. The SEM picture of the nanoporous alumina sample A30 from a surface (a) and a side view (b). The size of pores and a period of the array were similar for all the investigated samples. Since it was hard to mount the sample perfectly aligned to the electron beam during the characterization, one of the side surfaces can be seen in the image (gray color).

A direct 2 MeV He^+ beam (the sample was removed) backscattered from the gold layer produced a sharp peak in spectra measured by Detector 2. A peak at the same energy was also observed when the sample was aligned (Fig. 3(a)).

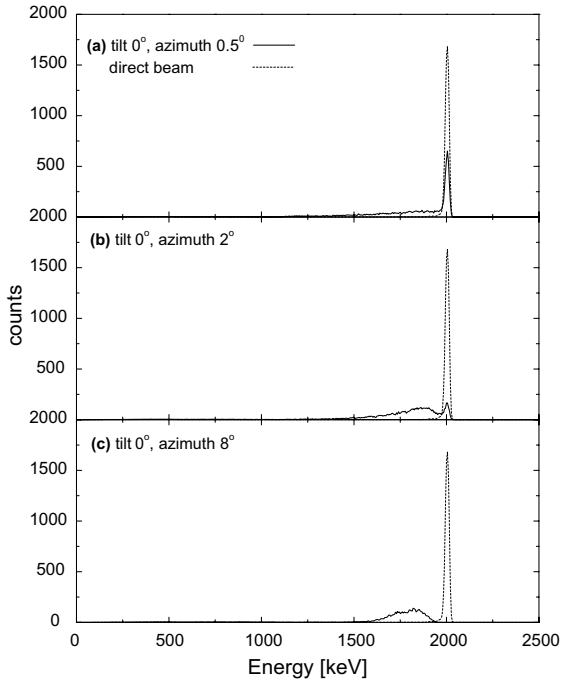

Fig. 3. Energy spectrum of transmitted beam through the sample A30 at three different orientations. The tilt and azimuth angle are measured from the initial position of the target wheel, nearly perpendicular to the beam. The width of the transmission peak (~20 keV) is comparable with the detector resolution.

This indicates that a substantial part of the beam passes through the pores without energy loss. When the sample is misaligned (Fig. 3(b,c)), the number of directly transmitted ions decreases, but a larger number of ions appears at lower energies. To align the sample with respect to the incident beam, the number of counts in the transmission peak (energy range between 1980 and 2030 keV) was recorded at different orientations. The angular scan was done in steps of 0.5 degrees for tilt and azimuth angles. The acquisition time at each position was 15 s. The results for 2 and 7 μm thick samples A30 and A31 respectively are shown in Fig. 4. The acceptance angle for transmission through pores α_0 was determined as the full width at half maximum (FWHM) of the peak projection on the tilt axis. The ion transmission was defined as the ratio between the transmitted current at the aligned orientation and the direct current measured when the sample was removed.

Characteristics of the investigated samples are summarized in Table 1. In general, higher transmission was obtained for thinner membranes, but differences were observed for samples of the same thickness and even for membrane pieces from the same alumina foil. The acceptance angle was larger for samples with better transmission. Samples marked with asterisk A27b* and A30* were covered with an approximately 10 nm thin gold layer in order to check possible influences of sample surface charging. From the results it can be concluded that this did not have a significant influence on transmission.

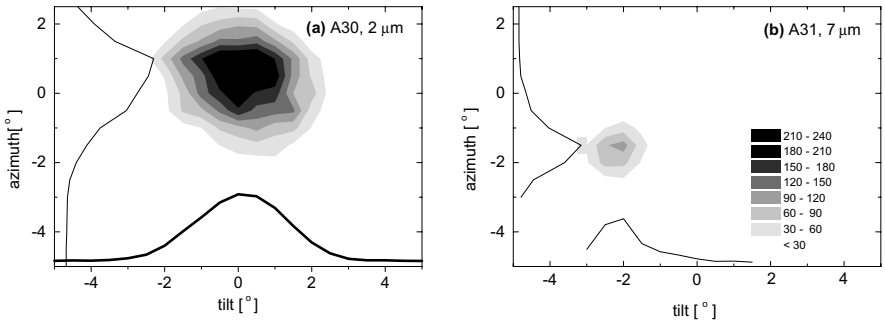

Fig. 4. Angular scans of the transmission through the pores for the 2 μm thick sample A30 (a) and the 7 μm thick sample A31 (b). Both angles were measured from the zero position of the target holder set perpendicular to the incident beam. The solid lines are projections of the peak on the tilt and azimuth axes in arbitrary units.

Table 1
Properties of the investigated samples

Sample	Thickness (μm)	Transmission (%)	α_0 (°)
A20a	10	0.7 ± 0.1	1.0
A20b	10	0	0
A23	2	4 ± 0.5	1.7
A27a	2	21 ± 3	1.6
A27b*	2	47 ± 5	2.3
A30	2	40 ± 5	2.4
A30*	2	50 ± 5	2.7
A31	7	22 ± 3	1.3
A39a	2	31 ± 4	1.6
A39b – reetched	2	64 ± 8	4.0

The samples were marked by the letter A and two digit numbers. Additional letters a and b refer to different pieces taken from the same foil. The asterisk indicates that the sample was covered with a thin gold layer. The sample A30 was studied first without and then with a gold layer. A SEM image of A39a showed that the pore ends were not completely open, so the second piece from this membrane A39b was etched longer in 5% H_3PO_4 solution.

For the sample A39a, where 1 h of etching in H_3PO_4 solution was not sufficient to open the pores after anodization, there are two peaks at the energies 2000 and 1150 keV observed in the transmission spectrum at the aligned orientation (Fig. 5(a)). After additional etching the lower energy peak shifts to higher energy (~1860 keV) and becomes broader (Fig. 5(b)). Transmission through pores improved from 31% to 64% for the aligned sample and the acceptance angle was increased as well from 1.6° to 4.0°.

Energy spectrum of transmitted O^+ beam with the incident energy of 3 MeV through the aligned sample A30* is displayed in Fig. 6. The transmission is comparable to the value obtained for the He^+ ions within the experimental error. It can be seen that only one peak is present in the spectrum, which means that the mask thickness is sufficient to stop ions hitting the solid material.

The standard RBS spectrum of the sample A30* acquired by Detector 1 at the aligned and misaligned orientation (8° in azimuth from aligned position) is shown in Fig. 7. The signal from the thin gold layer was used for ion fluence calibration. The peak close to the channel 130 appears in the spectra due to overlap of aluminum and oxygen scattering contributions. Unlike in the experiments of Pesiri et al. [7], a channeling-like decrease in yield at the aligned compared to the misaligned orientation can be observed. The effect was present also in RBS spectra of the 7 μm thick sample A31 at channels corresponding to

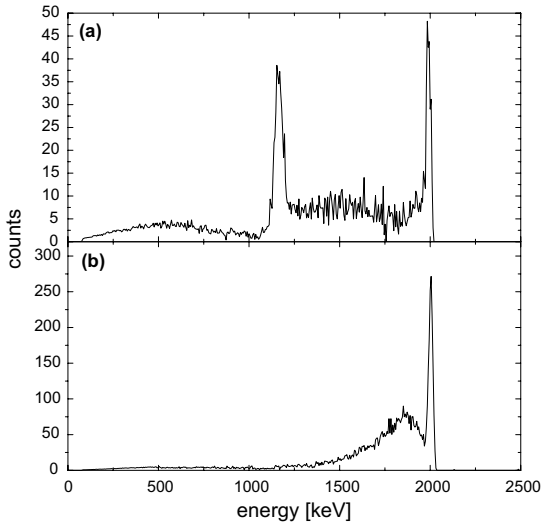

Fig. 5. Transmission energy spectrum of the samples A39a (a) and A39b (b) taken from the same alumina membrane. Bottoms of the pores at the piece A39a were not completely open, therefore the sample A39b was exposed to additional etching in H_3PO_4 solution. It can be seen that the low energy peak corresponding to transmission through the solid material is broader and shifted to higher energy ~1860 keV (b).

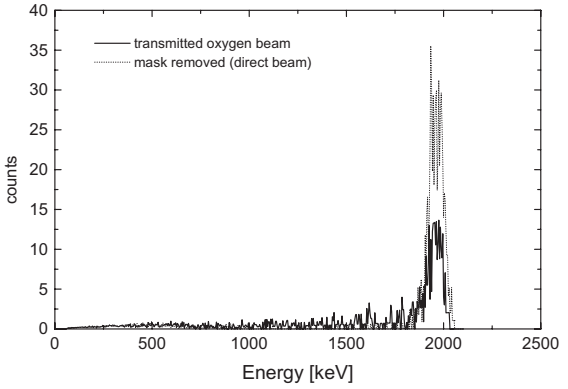

Fig. 6. Comparison between the energy spectrum of the transmitted O^+ beam through the sample A30* and the energy distribution measured with a sample removed. The resolution of these spectra is limited by the thickness of Au foil used in the detection system (Fig. 1).

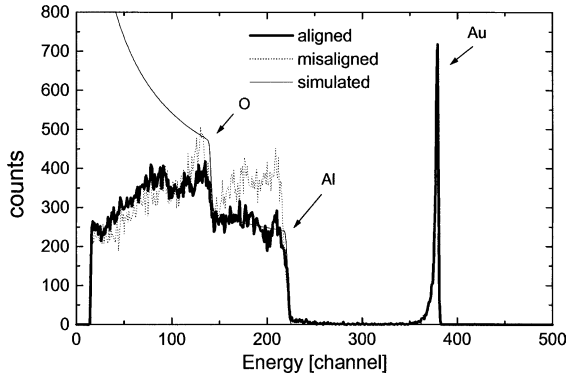

Fig. 7. RBS spectra of the 2 μm thick sample A30* at the aligned and misaligned orientation (8° from the aligned position in azimuth). The peak corresponding to scattering on a thin gold coating was used for ion fluence calibration needed for comparison between measurements. The solid line is a result of SIMNRA simulation for a 2 μm thick Al_2O_3 sample.

scattering near the surface. The thin solid line in Fig. 6 shows the simulated spectrum calculated by SIMNRA code [8] for 2 μm thick homogenous Al_2O_3 film. Although the stoichiometry of the real samples might be slightly different, discrepancy between simulated and experimental data cannot be assigned only to the atomic composition. The yield in the measured spectra at the energies related to scattering from larger depths of the sample is much lower than expected.

4. Discussion

A simplified geometry of a porous film can be seen in Fig. 8. The acceptance angle is defined as $\alpha_0 = \arctan b/d \approx b/d$, where b is the distance between solid walls and d the sample thickness. If the distance b is assumed to be 70 nm, the values of α_0 are 2° and 0.6° for 2 and 7 μm thick samples, respectively. The expected maximum ion transmission can be estimated as a relative surface area covered by pores (surface porosity) which is approximately 45% in our case. A comparable value to this prediction was measured for some of the 2 μm thick foils, although the results showed strong dependence on sample quality. Since all of the films were very thin, it was hard to keep their surface perfectly flat when mounting them to the brass frame. This probably explains the difference between transmission of samples A27a and A27b* taken from the same piece of alumina membrane. A slight bending of the surface and cracking of the foil was also observed after several hours of beam irradiation by the current of few nanoamperes.

From the energy spectra for sample A30 it can be seen that the width of the transmission peak is equal to the direct beam (Fig. 3). This means that a significant part of the pores is completely open and that their angular distribution with respect to the beam direction is small compared to the acceptance angle. Since the energy of the impinging beam is large enough to penetrate the solid material, there are two peaks expected in the transmission spectrum recorded by Detector 2 at the aligned orientation (Fig. 5(a)). The first one at the energy E corresponds to ions passing the pore with no energy loss (Fig. 9(a)) and the second one at the energy $E - \Delta E_1$ to those passing the solid material (Fig. 9(b)), where ΔE_1 is the average energy loss in the material (~1000 keV for a 2 μm thick Al_2O_3

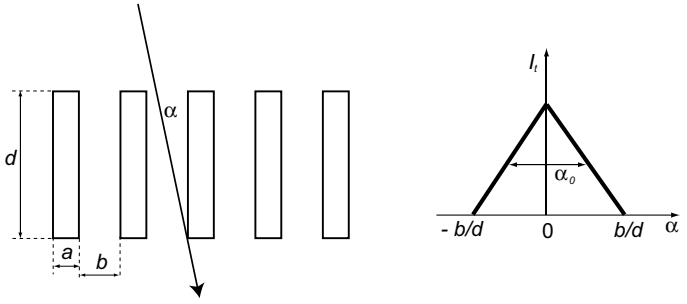

Fig. 8. A simplified model of nanoporous alumina and the expected angular dependence of transmitted current on the energy of the incident beam. The acceptance angle α_0 is defined as FWHM of the peak.

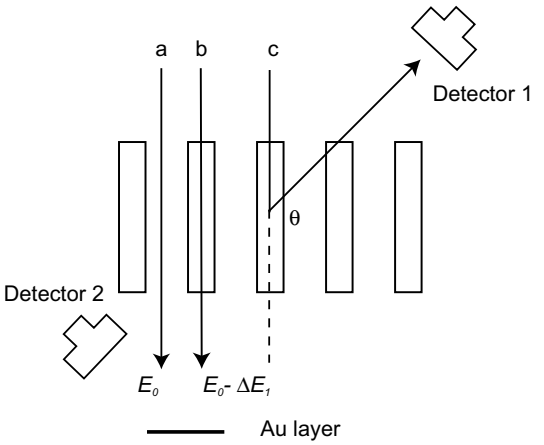

Fig. 9. Ion transmission through pores (a), solid material (b) and backscattering (c) at the aligned orientation of an ideal sample.

sample) [9]. Except for the sample A39a with partially closed pore ends, the second peak was observed at higher energies than expected. This indicates that the average atomic surface density in the solid material between pores is smaller in comparison to the bulk material of the same thickness. A long tail part in the transmission spectra also means that the material density is distributed within a large interval. When the sample A30 is turned for 8° from the aligned orientation, transmitted ions form a broad peak at the energy ~1800 keV (Fig. 3(c)). If the effective atomic density ρ_{eff} of a porous film is defined as the equivalent atomic density of homogenous solid material resulting in the same average energy loss for ions, ρ_{eff} for the sample A30 is only about 20% of the value for the 2 μm thick homogenous Al_2O_3 target.

The broad distribution of ρ_{eff} for the investigated samples can be explained by non-uniform thickness of pore walls. From comparison of the transmission spectra for samples A39a and A39b before and after additional etching in the H_3PO_4 solution it can be concluded that some of the solid material is removed (Fig. 10). This results in a shift of the low energy peak in transmission spectra (Fig. 5). The acceptance angle for the reetched sample is larger as well, which means that the pores increased after the procedure. The differences between this and the rest of the samples suggest that the etch rate is very sensitive to the sample composition which might result in non-uniform wall thickness.

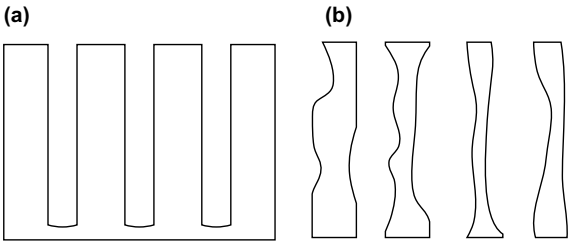

Fig. 10. Simplified sketch showing the influence of etching in the H_3PO_4 solution on the sample structure. The procedure opens the pore ends after the anodization steps, but also removes solid material along the wall.

A similar conclusion follows from the backscattering results using Detector 1. The spectrum measured for the sample A30* moved 8° from the aligned orientation (Fig. 7) does not match with a simulated result for 2 μm thick Al_2O_3 bulk target with the atomic surface density of 230×10^{17} atoms/cm^2. Better agreement is achieved for the SIMNRA simulation shown in Fig. 11, where the target was described as Al_xO_y with $x = 1$ and $y = 2$ rather than $x = 2$ and $y = 3$, and the non-uniform effective atomic surface density with the average

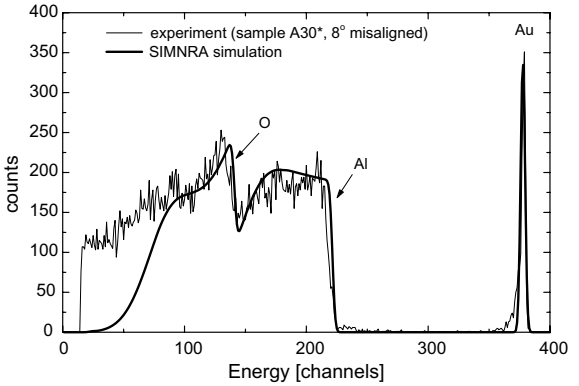

Fig. 11. Experimental and simulated RBS spectrum for the sample A30* tilted 8° from the aligned direction. The simulation was performed by the SIMNRA code. The effective atomic surface density with an average value of 55×10^{17} atoms/cm^2 and FWHM of 30×10^{17} was assumed. A better agreement was achieved for AlO_2 rather than Al_2O_3 sample composition.

value $\langle \rho_{\text{eff}} \rangle = 55 \times 10^{17}$ atoms/cm^2 and FWHM of 30×10^{17} atoms/cm^2. The details of the SIMNRA calculations for targets with non-uniform thickness are discussed in [10]. The effective atomic surface density of the thin gold layer on the alumina foils was assumed to be 5×10^{15} atoms/cm^2. The aluminum surface edge and the gold peak in simulated spectra do not completely fit the experimental data in Fig. 11. A probable reason is that a small amount of gold has entered into the pores [7]. In spite of that, the presented analysis of RBS and transmission measurements both suggest that ρ_{eff} of investigated samples has a broad distribution and about four to five times lower average value than the bulk alumina.

We have not simulated the RBS spectra in the aligned orientation, since different atomic surface densities in the target must be considered before and after scattering (Fig. 9(c)). A detailed study of channeling-like effects in porous materials was done on the basis of Monte Carlo simulations by Pászti and Szilágyi [11]. The same group also observed and analyzed channeling-like effects in porous silicon and reported a good agreement between simulated and experimental results [12].

5. Conclusions

Our results provide information about nanoporous alumina membranes. The ion transmission is an individual characteristic of each sample to some extend due to different mounting, but mainly due to pore quality. However, the maximum transmission of 2 μm thick membranes was between 30% and 65%, which is comparable to the relative surface area covered by pores. An alignment procedure presented in this paper is required to optimize transmission.

It was concluded from results of transmission studies and conventional RBS that the effective atomic surface density of investigated material is about four to five times lower than for bulk Al_2O_3 (not about twice as expected from surface porosity) and has a broad distribution due to differences in the solid wall thickness. The presented results show that one of the sources for this characteristic is the etching procedure after two step anodization. Since the etch rate is highly sensitive to sample composition of the initial high purity aluminum which is hard to control, mask quality could be improved if this step was replaced by an alternative method.

In conclusion, it can be seen from the presented experiments with a 3 MeV O^+ beam, that the effective atomic surface density of 2 μm thick nanoporous alumina is sufficient to completely stop the ions which hit the walls of the porous alumina. It means that the samples are promising templates for pattern transfer by MeV ion lithography. At the present step of the project, the irradiation process and selective chemical etching of different materials are being in progress for this application.

Acknowledgements

A part of this research was supported by the Commission of the European Community in the framework of Research and Training Network EuNITT, Contract no. HPRN-CT-2000-00047. The authors would also like to thank Mohamed Abid for his valuable input to the project.

References

[1] H. Masuda, K. Nishio, N. Baba, Jpn. J. Appl. Phys. 31 (1992) L1775.
[2] A. Hucko, Appl. Phys. A 70 (2000) 365.
[3] H. Masuda, K. Fukuda, Science 268 (1995) 1466.
[4] N. Matsuura, T.W. Simpson, I.V. Mitchell, X.Y. Mei, P. Morales, H.E. Ruda, Appl. Phys. Lett. 81 (2002) 4826.
[5] L.E. Rehn, B.J. Kestel, P.M. Baldo, J. Hiller, A.W. McCormick, R.C. Birtcher, Nucl. Instr. and Meth. B 206 (2003) 490.
[6] C.R. Martin, Science 266 (1994) 1961.
[7] D.R. Pesiri, R.C. Snow, N. Elliott, C. Maggiore, R.C. Doyle, J. Membrane Sci. 176 (2000) 209.
[8] M. Mayer, SIMNRA user's guide. Tech. Rep. IPP 9/113, Max-Planck-Institut für Plasmaphysik, Garching, 1997.
[9] J.F. Ziegler, J.R. Biersack, U. Littmark, The Stopping and Ranges of Ions in Matter, Vol. 1, Plenum Press, New York, 1985, Available from www.srim.org.
[10] M. Mayer, Nucl. Instr. and Meth. B 194 (2002) 177.
[11] F. Pászti, E. Szilágyi, Vacuum 50 (1998) 451.
[12] Z. Hajnal, E. Szilágyi, F. Pászti, G. Battistig, Nucl. Instr. and Meth. B 118 (1996) 617.